

# Unmanned Aerial Transportation System With Flexible Connection Between the Quadrotor and the Payload: Modeling, Controller Design, and Experimental Validation

Xiao Liang<sup>ID</sup>, Member, IEEE, Hai Yu<sup>ID</sup>, Zhuang Zhang, Huawang Liu<sup>ID</sup>, Yongchun Fang<sup>ID</sup>, Senior Member, IEEE, and Jianda Han<sup>ID</sup>, Member, IEEE

**Abstract**—Aerial delivery is becoming a reality due to the development of microelectronics and communication technology. Most existing methods for cable-suspended transportation systems utilize fixed-length cable to connect the unmanned aerial vehicle quadrotor and the payload. Such aerial transportation systems present underactuated property, which is caused by the indirectly controllable payload motion and the underactuation of the quadrotor itself. In practical applications, payload hoisting and lowering motion independent of the quadrotor altitude will further expand the application scope in such areas as limited space crossing and offshore sample collection. To realize the aforementioned objectives, a flexible connection between the quadrotor and the payload is realized by mounting an actuator beneath the fuselage. Suffering from strong nonlinearity and complex dynamic coupling, the control problem becomes extremely challenging and more cumbersome, as the system's degree of freedom (DOF) increases. To deal with these problems, in this article, a nonlinear control approach is presented by energy-based analysis, which achieves simultaneous quadrotor positioning, payload swing elimination and hoisting/lowering. Lyapunov techniques and LaSalle's Invariance theorem are utilized to prove the asymptotic convergence of the equilibrium point. Finally, a series of hardware experiments are conducted on a self-built aerial transportation platform. As far as we know, this article provides the first mechanism and control solution for payload hoisting/lowering independent of the quadrotor altitude.

Manuscript received 21 April 2021; revised 16 July 2021 and 5 January 2022; accepted 18 March 2022. Date of publication 5 April 2022; date of current version 5 October 2022. This work was supported in part by the National Natural Science Foundation of China under Grant 61903200, Grant 61873132, and Grant 91848203, in part by the Natural Science Foundation of Tianjin under Grant 19JCQNJC03500, in part by the Young Elite Scientists Sponsorship Program by Tianjin under Grant TJSQNTJ-2020-21. (Corresponding authors: Yongchun Fang and Jianda Han.)

The authors are with the College of Artificial Intelligence and Tianjin Key Laboratory of Intelligent Robotics, Institute of Robotics and Automatic Information Systems, Nankai University, Tianjin 300350, China (e-mail: liangx@nankai.edu.cn; yuhai@mail.nankai.edu.cn; zhangzhuang@mail.nankai.edu.cn; huawangl@nankai.edu.cn; fangyc@nankai.edu.cn; hanjianda@nankai.edu.cn).

This article has supplementary material provided by the authors and color versions of one or more figures available at <https://doi.org/10.1109/TIE.2022.3163526>.

Digital Object Identifier 10.1109/TIE.2022.3163526

**Index Terms**—Aerial transportation systems, Lyapunov techniques, payload hoisting/lowering, swing elimination.

## I. INTRODUCTION

WITH the rapid development of the logistics industry, it is gradually becoming a great demand to implement express deliveries with robotic techniques. Thanks to the high maneuverability and the flexibility of quadrotor unmanned aerial vehicles (UAVs) [1]–[6], it is an ideal way to employ the quadrotor for various transportation tasks. Aerial transportations could offer access to regions that are unreachable for ground vehicles, thus, many research efforts have been made for such tasks as forest fire fighting, oil and gas spill detection, search-and-rescue, etc. In the latest decade, some published works have adapted grippers [7]–[9], manipulators [10]–[12], and suspending cables [13]–[15] to complete transportation works. Usually, grippers and manipulators are mostly applied in payload operation tasks, yet it is difficult to transport large cargoes due to the limited size of the end effector. Moreover, the cable-suspended way is a low-cost transportation manner as it saves the development cost of the gripper and the manipulator.

Generally, a quadrotor possessing six degrees of freedom (DOFs), yet only four inputs, is a kind of underactuated system. Two additional DOFs are added to the system because of the payload's swing during flight [16]–[18], which increases the underactuated degree of the system. With complicated dynamics in state coupling and nonlinearity, some investigations have been done on underactuated aerial transportation systems with fixed-length cable. For these systems, there are two typical categories to handle the payload dynamics that cannot be controlled directly. In some researches, the quadrotor UAV was modeled individually, while the payload was treated as the disturbance [19]–[21]. Guo *et al.* [19] presented a multiple observers-based antidisturbance control scheme for a quadrotor against both cable-suspended payload disturbance and wind disturbance. Besides, to reduce the payload oscillation, the disturbance observer-based controller was designed in the translational control loop. In addition, a nonlinear extended state observer was designed for quadrotor's inner loop subsystem [20],

which enabled the system to achieve attitude stabilization with the payload suspended in one side of the quadrotor. To minimize the effect of the suspended unknown payload on the quadrotor, a robust model reference adaptive control method was presented in [21]. Nevertheless, accurate system dynamic models with consideration of payload sway are the basis of high-performance control, particularly, in payload swing elimination. Newton–Euler approach was utilized to obtain the aerial transportation system model in [22]. Specifically, the system was modeled in three discrete states: setup, pull, and raise. In [23], Lagrangian mechanics was applied to establish the system model.

To achieve accurate positioning and payload swing suppression, a number of control schemes have been designed and applied to cable-suspended aerial transportation systems in recent years. In [24] and [25], the additional input shaper to the controller could reduce the maximum and the residual payload swing during repositioning maneuver, by which the antiswing effect was much improved without significant additional time consumption. A mixed integer quadratic program trajectory planning method for the quadrotor flying in a known obstacle-filled environment was presented in [26] by constructing a hybrid dynamical model. An iterative linear quadratic regulator (iLQR) optimal controller was designed for the cable-suspended system [27]. Compared with the LQR controller, the quadrotor's aggressive trajectory tracking ability was improved. Based on Pontryagin's minimum principle, Hashemi *et al.* [28] adopted the indirect method to optimize and obtain the optimal trajectory that could improve the carrying capacity and reduce the oscillation of the payload. In [29], an interconnection and damping assignment-passivity-based control was proposed to transport the payload from point to point. A nonlinear adaptive control strategy was designed with a satisfactory antiswing performance [30], which reduced overshoots and suppressed payload swing more effectively. In addition to the studies on the aerial transportation system consisting of a single quadrotor with one payload, there were also several other types of transportation forms [31]–[33]. Chen *et al.* [31] studied the transportation form with one quadrotor and four cables. A tilt-rotor was utilized to pull an unmodeled cart through a thin cable in [32]. To avoid singularities and complexities, a geometric nonlinear PID controller was designed for the aerial transportation system with arbitrary number of quadrotors in a coordinate-free fashion, which made the payload asymptotically follow a given desired trajectory under uncertainties [33].

However, existing researches are most on the aerial transportation systems with fixed-length cable, thus the payload's hoisting/lowering motion can only be achieved by changing the height of the quadrotor. In some specific scenarios, the fixed-length cable transportation way cannot meet the demand in limited space crossing or offshore sample collection. Specifically, the quadrotor or the payload may hit the obstacle while crossing through the cave with the fixed-length cable. Therefore, shortening the cable length before traversing the cave makes the flight process feasible. Though an optimal control method has been designed to drive the quadrotor with a payload suspended by a fixed-length cable to pass through a window [34], it is not qualified for such tasks if the cave becomes longer. Furthermore,

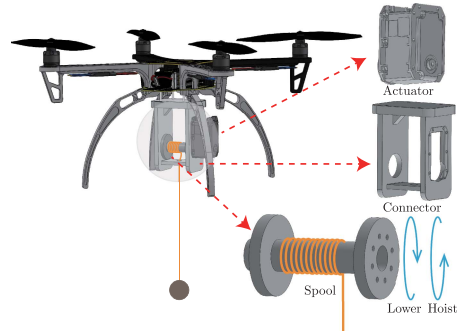


Fig. 1. Flexible connection mechanism for the aerial transportation system.

in order to pass through the narrow window, the quadrotor needs large instantaneous energy to wiggle the payload to swing up, so as to reduce the longitudinal relative distance between the fuselage and the payload. Nevertheless, such aggressive motion puts forward high requirements on the material and dynamic performance of the quadrotor, and brings extremely high-speed movement with great risk. For offshore sample collection tasks, considering the uncertainty of sea waves, the quadrotor must keep a long enough safe distance from the surface of the sea; to end this, one has to lengthen the cable before sampling. To realize the relative position adjustment between the payload and the quadrotor, while making the system more agile and maneuverable, a flexible connection between the quadrotor and the payload is in urgent need.

In this article, the aerial transportation system with payload hoisting/lowering ability is devised by mounting an actuator beneath the quadrotor. With the additional actuator and the corresponding mechanism, the cable length can be adjusted during flight according to the requirement, which expands the application scope of the aerial transportation system to more scenarios, especially for tasks in complex terrains. As shown in Fig. 1, the connection mechanism is formed by a spool, an actuator, and a connector. The spool is connected to the actuator through the connector, and the actuator could provide different driving torque to make the spool rotate in different directions. Specifically, when the spool rotates clockwise, the cable is released, so the cable length between the quadrotor and the payload becomes longer and the payload is lowered. On the contrary, when the spool rotates counterclockwise, the cable will be pulled back. At this time, the cable length between the quadrotor and the payload becomes shorter and the payload is hoisted. As the length of the cable can be adjusted, the number of state DOFs and control inputs of the system are increased, which implies that the underactuated system possesses nine DOFs and five control inputs. Compared with the aerial transportation systems with a fixed-length cable, the discussed case presents much stronger nonlinearity and more complex dynamic coupling due to the varying-length cable. Consequently, the control problem becomes even more complicated with consideration of payload hoisting and lowering. Based on the cascade characteristics of the system, we divide the system into two subsystems: the inner loop subsystem and the outer loop subsystem. The inner loop

subsystem is the rotation of the quadrotor, while the outer loop subsystem is composed of the translation of the quadrotor and the motion of the suspended payload connected by the actuator. To handle the aforementioned issues, the energy-based analysis method is utilized to construct a virtual control input, from which the applied quadrotor thrust and the force of the actuator are derived. Subsequently, the stability of the closed-loop system is guaranteed by Lyapunov techniques and LaSalle's Invariance theorem. Finally, through the proposed closed-loop control scheme, the performance of the developed aerial transportation system with flexible connection between the quadrotor and the payload is verified by several convincing experimental tests. The main contributions of this article are as follows:

- 1) Different from previous work on aerial transportation systems with fixed-length cable, this article provides the first complete design of the flexible connection mechanism, which could realize the payload hoisting and lowering by changing the distance between the quadrotor and the payload, and thus, greatly extend the application scope for different tasks.
- 2) Existing researches are aimed at the object with fixed-length cable, and there lacks the mechanism device to adjust the distance between the quadrotor and the payload, so those methods are built without the design for the cable length adjustment. For the aerial transportation system with a flexible connection between the quadrotor and the payload, it presents much stronger nonlinearity and more complex dynamic coupling owing to the varying-length cable dynamics. To this end, a nonlinear controller is proposed based on mechanical energy analysis without any linearization operations, which can drive the quadrotor position and the cable length to the desired state while suppressing the payload swing. Furthermore, the developed system achieves asymptotic stability as guaranteed by Lyapunov techniques and LaSalle's Invariance theorem.
- 3) The obtained experimental results show that the proposed control method has a better antiswing ability compared with the proportional-derivative (PD) controller and it is practicable for different traffic scenes even under disturbances.

The rest of this article is organized as follows. The dynamic model of the aerial transportation system with payload hoisting/lowering is established in Section II, where some characteristics are analyzed. The controller design process, as well as the stability analysis, is provided in Section III. In Section IV, several groups of experimental results are provided to show the performance of the control system. Finally, Section V concludes this article.

## II. DYNAMICS MODELING

The schematic configuration of a quadrotor transportation system with an actuator to hoist/lower the payload is shown in Fig. 2. Fixed at the bottom of the quadrotor, the actuator drives the spool to adjust the length of the cable.  $\{\mathcal{I}\}$  represents a right-hand inertia frame and  $\{\mathcal{B}\}$  is the body-fixed frame. The origin of the body-fixed frame is located at the quadrotor's

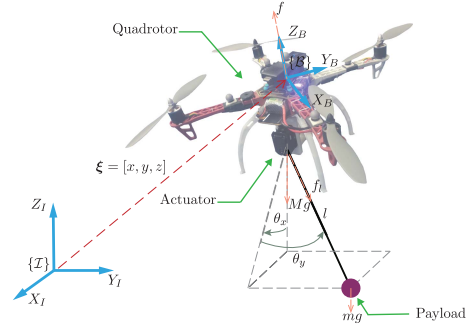


**Fig. 2.** Aerial transportation system with an installed actuator to hoist/lower the payload.

**TABLE I**  
SYMBOLS AND DEFINITIONS OF THE SYSTEM

Symbol	Definition
$M \in \mathbb{R}$	Mass of quadrotor
$m \in \mathbb{R}$	Mass of payload
$g \in \mathbb{R}$	Gravitational acceleration
$J \in \mathbb{R}^{3 \times 3}$	Quadrotor's moment of inertia
$R \in SO(3)$	Rotation matrix from $\{\mathcal{B}\}$ to $\{\mathcal{I}\}$
$Re_3 = [R_{13}, R_{23}, R_{33}]^\top$	Last column of rotation matrix $R$
$\xi = [x, y, z]^\top \in \mathbb{R}^3$	Quadrotor position in $\{\mathcal{I}\}$
$l \in \mathbb{R}$	Cable length
$\alpha = [\xi^\top, l]^\top \in \mathbb{R}^4$	Combination vector of quadrotor position and cable length
$\Theta = [\theta_x, \theta_y]^\top \in \mathbb{R}^2$	Payload swing angle
$q = [\alpha^\top, \Theta^\top]^\top \in \mathbb{R}^6$	Outer loop state vector
$\alpha_d = [x_d, y_d, z_d, l_d]^\top \in \mathbb{R}^4$	Desired quadrotor position and cable length
$q_d = [x_d^\top, 0, 0]^\top \in \mathbb{R}^6$	Desired state of outer loop subsystem
$\xi_p = [x_p, y_p, z_p]^\top \in \mathbb{R}^3$	Payload position in $\{\mathcal{I}\}$
$\Omega = [\Omega_1, \Omega_2, \Omega_3]^\top \in \mathbb{R}^3$	Angular velocity of quadrotor in frame $\{\mathcal{B}\}$
$\tau = [\tau_1, \tau_2, \tau_3]^\top \in \mathbb{R}^3$	Torque generated by quadrotor
$T_t \in \mathbb{R}$	Total kinetic energy of the system
$T_{ou} \in \mathbb{R}$	Kinetic energy of outer loop subsystem
$T_{in} \in \mathbb{R}$	Kinetic energy of inner loop subsystem
$P \in \mathbb{R}$	Gravitational potential energy
$M_c(q) \in \mathbb{R}^{6 \times 6}$	Inertia matrix
$V_c(q, \dot{q}) \in \mathbb{R}^{6 \times 6}$	Centripetal-Coriolis matrix
$G(q) \in \mathbb{R}^6$	Gravity vector
$u \in \mathbb{R}^6$	Outer loop control input vector
$f \in \mathbb{R}$	Applied thrust generated by quadrotor
$f_l \in \mathbb{R}$	Hoisting/lowering actuating force
$f_v = [f_{vx}, f_{vy}, f_{vz}]^\top \in \mathbb{R}^3$	Desired control input generated by quadrotor
$f_a \in \mathbb{R}^3$	Auxiliary signal (Error between $fRe_3$ and $f_v$ )
$f_{ou} = [f_v^\top, f_l]^\top \in \mathbb{R}^4$	Intermediate extended variable for $f_v$ and $f_l$
$f_{el} = [f_{ou}^\top, 0, 0]^\top \in \mathbb{R}^6$	Intermediate extended variable for $f_{ou}$
$f_{au} = [f_a^\top, 0, 0, 0]^\top \in \mathbb{R}^6$	Intermediate extended variable for $f_a$

center of mass. The symbols and the definitions are listed in Table I. Considering the actual transportation systems, as well as the recent researches [35]–[37], the following reasonable assumptions are given.

*Assumption 1:* The suspension cable is inelastic and massless.

*Assumption 2:* The payload is always under the quadrotor, implying that the swing angles  $\theta_x$  and  $\theta_y$  are within the range of  $(-\pi/2, \pi/2)$ .

From Fig. 2, according to geometric relations, one can first express the payload's position  $\xi_p(t) = [x_p(t), y_p(t), z_p(t)]^\top$  as follows:

$$\xi_p = [x + lS_x C_y, y + lS_y, z - lC_x C_y]^\top \quad (1)$$

where  $C_x$ ,  $C_y$ ,  $S_x$ , and  $S_y$  represent  $\cos(\theta_x)$ ,  $\cos(\theta_y)$ ,  $\sin(\theta_x)$ , and  $\sin(\theta_y)$ , respectively. Taking the time derivative of (1), one can obtain that

$$\dot{x}_p = \dot{x} + lS_xC_y + l\dot{\theta}_x C_x C_y - l\dot{\theta}_y S_x S_y \quad (2)$$

$$\dot{y}_p = \dot{y} + lS_y + l\dot{\theta}_y C_y \quad (3)$$

$$\dot{z}_p = \dot{z} - lC_x C_y + l\dot{\theta}_x S_x C_y + l\dot{\theta}_y C_x S_y. \quad (4)$$

The potential energy of the system including quadrotor and payload, is expressed as follows:

$$P = Mgz + mgz_p. \quad (5)$$

To facilitate the subsequent analysis, the total kinetic energy  $T_t$  is divided into two parts as  $T_t = T_{\text{in}} + T_{\text{ou}}$ , where  $T_{\text{ou}}$  contains the kinetic energy of the quadrotor translation and the payload motion,  $T_{\text{in}}$  is the rotation kinetic energy of the quadrotor, and the concrete expressions are provided as follows:

$$T_{\text{ou}} = \frac{1}{2} M \dot{\xi}^\top \dot{\xi} + \frac{1}{2} m \dot{\xi}_p^\top \dot{\xi}_p \quad (6)$$

$$T_{\text{in}} = \frac{1}{2} \Omega^\top J \Omega. \quad (7)$$

### A. Outer Loop Dynamic Modeling

The generalized coordinate of the outer loop subsystem is selected as  $\mathbf{q} = [\alpha^\top, \theta_x, \theta_y]^\top$ . The corresponding Lagrangian of the subsystem is given by

$$L_{\text{ou}} = T_{\text{ou}} - P. \quad (8)$$

The virtual work  $\delta W$  is expressed as  $\delta W = fR e_3 \cdot \delta \xi + f_l \cdot \delta l$ , wherein  $e_3 = [0, 0, 1]^\top$ . The generalized force can be obtained from the formula  $Q_k = \delta W / \delta q_k$ ,  $k = \{1, \dots, 6\}$  as follows:

$$Q_1 = fR_{13}, Q_2 = fR_{23}, Q_3 = fR_{33}, Q_4 = f_l, Q_5 = 0, Q_6 = 0. \quad (9)$$

According to the Lagrange's equation

$$\frac{d}{dt} \frac{\partial L_{\text{ou}}}{\partial \dot{q}_i} - \frac{\partial L_{\text{ou}}}{\partial q_i} = Q_i, i = \{1, \dots, 6\} \quad (10)$$

substituting (2)–(6), (8), and (9) into (10), the dynamic model of the outer loop subsystem can be obtained as follows:

$$\begin{aligned} & (M+m) \ddot{x} + ml \ddot{S}_x C_y + 2ml \dot{\theta}_x C_x C_y - 2ml \dot{\theta}_y S_x S_y + \\ & ml \left( \ddot{\theta}_x C_x C_y - \ddot{\theta}_y S_x S_y - \dot{\theta}_x^2 S_x C_y - \dot{\theta}_y^2 S_x C_y - 2\dot{\theta}_x \dot{\theta}_y C_x S_y \right) \\ & = fR_{13} \end{aligned} \quad (11)$$

$$\begin{aligned} & (M+m) \ddot{y} + ml \ddot{S}_y + 2ml \dot{\theta}_y C_y + ml \left( \ddot{\theta}_y C_y - \dot{\theta}_y^2 S_y \right) \\ & = fR_{23} \end{aligned} \quad (12)$$

$$\begin{aligned} & (M+m) \ddot{z} - ml \ddot{C}_x C_y + 2ml \dot{\theta}_x S_x C_y + 2ml \dot{\theta}_y C_x S_y + \\ & ml \left( \ddot{\theta}_x S_x C_y + \ddot{\theta}_y C_x S_y + \dot{\theta}_x^2 C_x C_y + \dot{\theta}_y^2 C_x C_y - 2\dot{\theta}_x \dot{\theta}_y S_x S_y \right) \\ & = fR_{33} - (M+m) g \end{aligned} \quad (13)$$

$$m \ddot{x} S_x C_y + m \ddot{y} S_y - m \ddot{z} C_x C_y + ml \ddot{l} - ml \dot{\theta}_x^2 C_y^2 - ml \dot{\theta}_y^2$$

$$- mg C_x C_y = f_l \quad (14)$$

$$ml \ddot{x} C_x C_y + ml \ddot{z} S_x C_y + ml^2 \dot{\theta}_x^2 C_y^2 + 2ml \dot{l} \dot{\theta}_x C_y^2$$

$$- 2ml^2 \dot{\theta}_x \dot{\theta}_y C_y S_y + mgl S_x C_y = 0 \quad (15)$$

$$- ml \ddot{x} S_x S_y + ml \ddot{y} C_y + ml \ddot{z} C_x S_y + ml^2 \ddot{\theta}_y + 2ml \dot{l} \dot{\theta}_y$$

$$+ ml^2 \dot{\theta}_x^2 C_y S_y + mgl C_x S_y = 0. \quad (16)$$

Further, collecting up (11)–(16), the following expression is derived:

$$M_c(\mathbf{q}) \ddot{\mathbf{q}} + V_c(\mathbf{q}, \dot{\mathbf{q}}) \dot{\mathbf{q}} + \mathbf{G}(\mathbf{q}) = \mathbf{u} \quad (17)$$

where the terms in  $M_c = [M_{cij}]$ ,  $V_c = [V_{cij}]$ ,  $\mathbf{G} = [G_j]$ ,  $\mathbf{u} = [u_j]$ ,  $i, j = \{1, \dots, 6\}$ , are explicitly provided as follows:

$$M_{c11} = M_{c22} = M_{c33} = M + m, M_{c44} = m$$

$$M_{c55} = ml^2 C_y^2, M_{c66} = ml^2, M_{c14} = M_{c41} = m S_x C_y$$

$$M_{c15} = M_{c51} = ml C_x C_y, M_{c16} = M_{c61} = -ml S_x S_y$$

$$M_{c24} = M_{c42} = m S_y, M_{c26} = M_{c62} = ml C_y$$

$$M_{c34} = M_{c43} = -m C_x C_y, M_{c35} = M_{c53} = ml S_x C_y$$

$$M_{c36} = M_{c63} = ml C_x S_y, V_{c14} = m \dot{\theta}_x C_x C_y - m \dot{\theta}_y S_x S_y$$

$$V_{c15} = ml C_x C_y - ml \dot{\theta}_x S_x C_y - ml \dot{\theta}_y C_x S_y$$

$$V_{c16} = -ml S_x S_y - ml \dot{\theta}_x C_x S_y - ml \dot{\theta}_y S_x C_y$$

$$V_{c24} = m \dot{\theta}_y C_y, V_{c26} = ml C_y - ml \dot{\theta}_y S_y$$

$$V_{c34} = m \dot{\theta}_x S_x C_y + m \dot{\theta}_y C_x S_y, V_{c64} = ml \dot{\theta}_y$$

$$V_{c35} = ml S_x C_y + ml \dot{\theta}_x C_x C_y - ml \dot{\theta}_y S_x S_y$$

$$V_{c36} = ml C_x S_y - ml \dot{\theta}_x S_x S_y + ml \dot{\theta}_y C_x C_y$$

$$V_{c45} = -ml \dot{\theta}_x C_y^2, V_{c46} = -ml \dot{\theta}_y, V_{c54} = ml \dot{\theta}_x C_y^2$$

$$V_{c55} = ml^2 \dot{\theta}_y S_y C_y, V_{c56} = -ml^2 \dot{\theta}_x C_y S_y$$

$$V_{c65} = ml^2 \dot{\theta}_x C_y S_y, V_{c66} = ml \dot{l}, G_3 = (M+m)g$$

$$G_4 = -mg C_x C_y, G_5 = mgl S_x C_y, G_6 = mgl C_x S_y$$

$$u_1 = fR_{13}, u_2 = fR_{23}, u_3 = fR_{33}, u_4 = f_l$$

and the left elements  $M_{c12}$ ,  $M_{c21}$ ,  $M_{c13}$ ,  $M_{c31}$ ,  $M_{c23}$ ,  $M_{c32}$ ,  $M_{c25}$ ,  $M_{c52}$ ,  $M_{c45}$ ,  $M_{c54}$ ,  $M_{c46}$ ,  $M_{c64}$ ,  $M_{c56}$ ,  $M_{c65}$ ,  $V_{c11}$ ,  $V_{c12}$ ,  $V_{c13}$ ,  $V_{c21}$ ,  $V_{c22}$ ,  $V_{c23}$ ,  $V_{c25}$ ,  $V_{c31}$ ,  $V_{c32}$ ,  $V_{c33}$ ,  $V_{c41}$ ,  $V_{c42}$ ,  $V_{c43}$ ,  $V_{c44}$ ,  $V_{c51}$ ,  $V_{c52}$ ,  $V_{c53}$ ,  $V_{61}$ ,  $V_{62}$ ,  $V_{63}$ ,  $G_1$ ,  $G_2$ ,  $u_5$ , and  $u_6$  are zeros.

### B. Inner Loop Dynamics Modeling

Due to the suspended way, the rotational dynamics of the quadrotor is not influenced by the payload. Thus, the inner loop subsystem stays the same as the situation without suspended payload, which is expressed by

$$\dot{R} = R \dot{\Omega} \quad (18)$$

$$J \dot{\Omega} + \Omega \times J \Omega = \tau \quad (19)$$

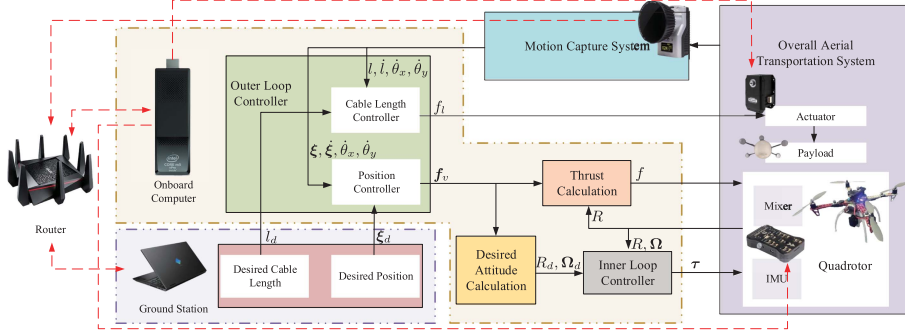


**Fig. 3.** Schematic of the control structure and the communication signal transmission. (Black solid lines: Control signals. Red dotted lines: Communication signals.)

where the hat map  $\hat{\cdot} : \mathbb{R}^3 \rightarrow \mathfrak{so}(3)$  is defined by the condition that  $\hat{x}\hat{y} = \hat{x}y + x\hat{y}$  for all  $x, y \in \mathbb{R}^3$ . The inverse of the hat map is expressed by the vee map  $\vee : \mathfrak{so}(3) \rightarrow \mathbb{R}^3$ .

### C. Model Analysis

Based on the aforementioned derivations, the complete model of the system can be summarized by (17)–(19). It can be proven that the outer loop subsystem (17) satisfies the following important properties without much difficulty.

*Property 1:* Matrix  $M_c(\boldsymbol{q})$  is positive definite.

*Property 2:* Matrices  $V_c(\boldsymbol{q}, \dot{\boldsymbol{q}})$  and  $M_c(\boldsymbol{q})$  satisfy the skew-symmetric relationship:  $\boldsymbol{\eta}^\top (\frac{1}{2}M_c - V_c)\boldsymbol{\eta} = 0, \forall \boldsymbol{\eta} \in \mathbb{R}^6$ .

## III. CONTROLLER DESIGN AND STABILITY ANALYSIS

The control objective of this article is to design the applied force  $\boldsymbol{u}$  generated by the outer loop subsystem, and the torque  $\boldsymbol{\tau}$  generated by the inner loop subsystem, so as to drive the quadrotor and the cable from their initial states  $\boldsymbol{\alpha}_0$  to the desired states  $\boldsymbol{\alpha}_d$ , while suppressing the payload swing  $\boldsymbol{\Theta}$  in the following sense:

$$\boldsymbol{q} = [\boldsymbol{\alpha}^\top, \boldsymbol{\Theta}^\top]^\top \rightarrow \boldsymbol{q}_d = [\boldsymbol{\alpha}_d^\top, 0, 0]^\top.$$

Fig. 3 shows the control structure and the communication signal transmission of the system.

### A. Controller Design

To facilitate the subsequent controller development and analysis, define the error vector  $\boldsymbol{e}_\alpha = \boldsymbol{\alpha}(t) - \boldsymbol{\alpha}_d = [e_x(t), e_y(t), e_z(t), e_i(t)]^\top \in \mathbb{R}^4$ . Then, the outer loop error  $\boldsymbol{e}_q \in \mathbb{R}^6$  is defined as

$$\boldsymbol{e}_q = \boldsymbol{q} - \boldsymbol{q}_d = [\boldsymbol{e}_\alpha^\top, \boldsymbol{\Theta}^\top]^\top \quad (20)$$

and the quadrotor's attitude and angular velocity tracking errors [38], i.e.,  $\boldsymbol{e}_R(t), \boldsymbol{e}_\Omega(t) \in \mathbb{R}^3$ , are defined as

$$\boldsymbol{e}_R = \frac{1}{2} (R_d^\top \boldsymbol{R} - \boldsymbol{R}^\top R_d)^\vee \quad (21)$$

$$\boldsymbol{e}_\Omega = \boldsymbol{\Omega} - \boldsymbol{R}^\top R_d \boldsymbol{\Omega}_d. \quad (22)$$

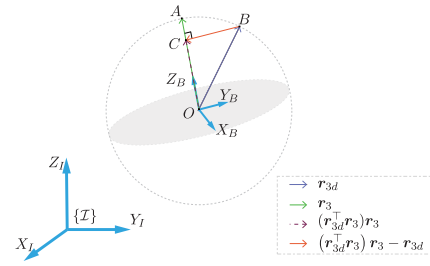


**Fig. 4.** Diagram of vectors  $fRe_3$ ,  $f_a$ , and  $f_v$ .

After some calculations through (18)–(22), the time derivatives of  $\boldsymbol{e}_q(t)$ ,  $\boldsymbol{e}_R(t)$ , and  $\boldsymbol{e}_\Omega(t)$  are given as

$$\dot{\boldsymbol{e}}_q = [\dot{\boldsymbol{e}}_\alpha^\top, \dot{\boldsymbol{\Theta}}^\top]^\top = \dot{\boldsymbol{q}} \quad (23)$$

$$\dot{\boldsymbol{e}}_R = \frac{1}{2} (\boldsymbol{R}_d^\top \boldsymbol{R} \dot{\boldsymbol{e}}_\Omega + \dot{\boldsymbol{e}}_\Omega \boldsymbol{R}^\top \boldsymbol{R}_d)^\vee \quad (24)$$

$$\dot{\boldsymbol{e}}_\Omega = \boldsymbol{\tau} - \hat{\boldsymbol{\Omega}} \boldsymbol{J} \boldsymbol{\Omega} + \boldsymbol{J} (\hat{\boldsymbol{\Omega}} \boldsymbol{R}^\top \boldsymbol{R}_d \boldsymbol{\Omega}_d - \boldsymbol{R}^\top \boldsymbol{R}_d \hat{\boldsymbol{\Omega}}_d). \quad (25)$$

From the outer loop input vector, it can be seen that the two subsystems are coupled through the rotation matrix  $\boldsymbol{R}(t)$ . To deal with the coupling term, define two unit vectors as  $\boldsymbol{Re}_3 = \boldsymbol{r}_3, \boldsymbol{R}_d \boldsymbol{e}_3 = \boldsymbol{r}_{3d}$ , and a scalar  $s = f / (\boldsymbol{e}_3^\top \boldsymbol{R}_d^\top \boldsymbol{Re}_3) = f / (\boldsymbol{r}_{3d}^\top \boldsymbol{r}_3)$ , then divide  $fRe_3$  into the following two parts:

$$fRe_3 = \underbrace{\frac{f}{\boldsymbol{e}_3^\top \boldsymbol{R}_d^\top \boldsymbol{Re}_3} ([\boldsymbol{e}_3^\top \boldsymbol{R}_d^\top \boldsymbol{Re}_3] \boldsymbol{Re}_3 - \boldsymbol{R}_d \boldsymbol{e}_3)}_{\boldsymbol{f}_a = s[(\boldsymbol{r}_{3d}^\top \boldsymbol{r}_3) \boldsymbol{r}_3 - \boldsymbol{r}_{3d}]} + \underbrace{\frac{f}{\boldsymbol{e}_3^\top \boldsymbol{R}_d^\top \boldsymbol{Re}_3} \boldsymbol{R}_d \boldsymbol{e}_3}_{\boldsymbol{f}_v = s \boldsymbol{r}_{3d}} \quad (26)$$

where  $\boldsymbol{f}_v = [f_{vx}, f_{vy}, f_{vz}]^\top \in \mathbb{R}^3$  denotes the desired control input of the quadrotor,  $\boldsymbol{f}_a \in \mathbb{R}^3$  denotes the auxiliary signal, which is the error between the actual force vector  $fRe_3$  and the desired control vector  $\boldsymbol{f}_v$ . To clarify the geometrical relationship between these vectors, a diagram is given as Fig. 4, whose coordinates are defined the same as Fig. 2. In Fig. 4, the center of the unit ball  $O$  is located at the quadrotor's center of mass. Define  $\overrightarrow{OA} = \boldsymbol{r}_3$  and  $\overrightarrow{OB} = \boldsymbol{r}_{3d}$ . Hence, one has  $(\boldsymbol{r}_{3d}^\top \boldsymbol{r}_3) \boldsymbol{r}_3 = \overrightarrow{OC}$ , which denotes the projection mapping of  $\boldsymbol{r}_{3d}$  onto  $\boldsymbol{r}_3$  with the same direction as  $\boldsymbol{r}_3$ . Besides, one knows  $(\boldsymbol{r}_{3d}^\top \boldsymbol{r}_3) \boldsymbol{r}_3 - \boldsymbol{r}_{3d} =$

$\overrightarrow{OC} - \overrightarrow{OB} = \overrightarrow{BC}$ . Thus, it is clear that  $\mathbf{f}_a$ ,  $\mathbf{f}_v$ , and  $fRe_3$  are  $s$  times as much as vector  $\overrightarrow{BC}$ ,  $\overrightarrow{OB}$ , and  $\overrightarrow{OC}$ .

Further, taking the time derivative of (23), and employing (17) and (26) yields

$$\begin{aligned}\ddot{\mathbf{e}}_q &= M_c^{-1} (\mathbf{u} - V_c \dot{\mathbf{e}}_q - \mathbf{G}) \\ &= M_c^{-1} \left( [\mathbf{f}_v^\top + \mathbf{f}_a^\top, f_l, 0, 0]^\top - V_c \dot{\mathbf{e}}_q - \mathbf{G} \right) \\ &= M_c^{-1} (\mathbf{f}_{vl} - V_c \dot{\mathbf{e}}_q - \mathbf{G}) + M_c^{-1} \mathbf{f}_{au}\end{aligned}$$

wherein  $\mathbf{f}_{vl} = [\mathbf{f}_{ou}^\top, 0, 0]^\top \in \mathbb{R}^6$ ,  $\mathbf{f}_{ou} = [\mathbf{f}_v^\top, f_l]^\top = [f_{vx}, f_{vy}, f_{vz}, f_l]^\top \in \mathbb{R}^4$ , and  $\mathbf{f}_{au} = [\mathbf{f}_a^\top, 0, 0, 0]^\top \in \mathbb{R}^6$ . From (26), one knows that  $\mathbf{f}_v$  and  $R_d e_3$  have the same direction, then the desired unit direction vector  $\mathbf{b}_{3d} = R_d e_3 \in \mathbb{R}^3$  can be obtained by

$$\mathbf{b}_{3d} = R_d e_3 = \frac{\mathbf{f}_v}{\|\mathbf{f}_v\|}. \quad (27)$$

Substituting (27) into  $\mathbf{f}_v$  yields

$$\mathbf{f}_v = \frac{f \|\mathbf{f}_v\|}{\mathbf{f}_v^\top R e_3} \frac{\mathbf{f}_v}{\|\mathbf{f}_v\|} = \frac{f \mathbf{f}_v}{\mathbf{f}_v^\top R e_3}$$

indicating that  $f = \mathbf{f}_v^\top R e_3$ .

Define a new outer loop error vector  $\mathbf{e}(t) = [\mathbf{e}_\alpha^\top(t), \dot{\mathbf{e}}_\alpha^\top(t)]^\top \in \mathbb{R}^{12}$ , and taking its time derivative, one obtains  $\dot{\mathbf{e}} = \kappa(\mathbf{e}, \mathbf{f}_{vl}, \boldsymbol{\alpha}_d) + \boldsymbol{\iota}$ , wherein  $\kappa \in \mathbb{R}^{12}$  and the coupling term  $\boldsymbol{\iota} \in \mathbb{R}^{12}$  take the form as

$$\kappa = \Pi_{10} \dot{\mathbf{e}}_\alpha + \Pi_{01} M_c^{-1} (\mathbf{f}_{vl} - V_c \dot{\mathbf{e}}_\alpha - \mathbf{G}), \boldsymbol{\iota} = \Pi_{01} M_c^{-1} \mathbf{f}_{au}.$$

The matrices  $\Pi_{10}, \Pi_{01} \in \mathbb{R}^{12 \times 6}$  are expressed as  $\Pi_{10} = [I_{6 \times 6}, 0_{6 \times 6}]^\top$  and  $\Pi_{01} = [0_{6 \times 6}, I_{6 \times 6}]^\top$ .

The energy function of the outer loop subsystem is given as

$$E = \frac{1}{2} \dot{\mathbf{q}}^\top M_c \dot{\mathbf{q}} + mgl (1 - C_x C_y). \quad (28)$$

Invoking *Property 2* and taking the time derivative of (28) leads to

$$\begin{aligned}\dot{E} &= \dot{\mathbf{q}}^\top \left( M_c \ddot{\mathbf{q}} + \frac{1}{2} \dot{M}_c \dot{\mathbf{q}} \right) + mgl \left( \dot{\theta}_x S_x C_y + \dot{\theta}_y C_x S_y \right) \\ &\quad + mg \dot{l} (1 - C_x C_y) \\ &= \dot{\mathbf{e}}_\alpha^\top \left( [f R e_3^\top, f_l]^\top - [0, 0, (M+m)g, -mg]^\top \right).\end{aligned}$$

Next, define the following auxiliary function:

$$E_s = \frac{1}{2} \mathbf{e}_\alpha^\top K_p \mathbf{e}_\alpha \quad (29)$$

where  $K_p = \text{diag}([k_{px}, k_{py}, k_{pz}, k_{pl}]) \in \mathbb{R}_+^{4 \times 4}$  is a positive definite diagonal matrix. According to (28) and (29), the total energy storage function is constructed as

$$V = E + E_s. \quad (30)$$

Taking the time derivative of (30) produces

$$\begin{aligned}\dot{V} &= \dot{\mathbf{e}}_\alpha^\top \left( [f R e_3^\top, f_l]^\top - [0, 0, (M+m)g, -mg]^\top + K_p \mathbf{e}_\alpha \right) \\ &= \dot{\mathbf{e}}_\alpha^\top \left( \mathbf{f}_{ou} + [\mathbf{f}_a^\top, 0]^\top - [0, 0, (M+m)g, -mg]^\top + K_p \mathbf{e}_\alpha \right).\end{aligned} \quad (31)$$

On the basis of (31), the following virtual control input is designed:

$$\mathbf{f}_{ou} = -K_p \mathbf{e}_\alpha - K_d \dot{\mathbf{e}}_\alpha + [0, 0, (M+m)g, -mg]^\top - \mathbf{f}_s \quad (32)$$

where  $K_d = \text{diag}([k_{dx}, k_{dy}, k_{dz}, k_{dl}]) \in \mathbb{R}_+^{4 \times 4}$  is a positive definite diagonal matrix.  $\mathbf{f}_s$  represents the payload swing signal injected into the controller, which increases state coupling between quadrotor and payload, and enhances the antiswing performance, constructed as

$$\mathbf{f}_s = K_s \left( \dot{\theta}_x^2 + \dot{\theta}_y^2 \right) \dot{\mathbf{e}}_\alpha \quad (33)$$

with  $K_s = \text{diag}([k_{sx}, k_{sy}, k_{sz}, k_{sl}]) \in \mathbb{R}_+^{4 \times 4}$  being a positive definite diagonal matrix.

*Remark 1:* In order to obtain the desired rotation matrix  $R_d(t)$ , after utilizing (27) to obtain the unit vector  $\mathbf{b}_{3d}$  and choosing an arbitrary vector  $\mathbf{b}_{1a}(t) \in \mathbb{R}^3$  not parallel to  $\mathbf{b}_{3d}$ , one can calculate the desired attitude as  $R_d = [\mathbf{b}_{2d} \times \mathbf{b}_{3d}; \mathbf{b}_{2d}; \mathbf{b}_{3d}]$ , where

$$\mathbf{b}_{2d} = \frac{\mathbf{b}_{3d} \times \mathbf{b}_{1a}}{\|\mathbf{b}_{3d} \times \mathbf{b}_{1a}\|}$$

represents the second row of the desired rotation matrix. For the desired attitude tracking problem, adopt the following control approach [38]:

$$\boldsymbol{\tau} = -K_R \mathbf{e}_R - K_\Omega \mathbf{e}_\Omega + \hat{\boldsymbol{\Omega}} J \boldsymbol{\Omega} - J \left( \hat{\boldsymbol{\Omega}} R^\top R_d \boldsymbol{\Omega}_d - R^\top R_d \dot{\boldsymbol{\Omega}}_d \right) \quad (34)$$

wherein  $K_R, K_\Omega \in \mathbb{R}_+^{3 \times 3}$  are positive definite diagonal matrices. Demonstrably, through the control law (34),  $\mathbf{e}_R(t)$  and  $\mathbf{e}_\Omega(t)$  converge to zero exponentially.

### B. Stability Analysis

Ignore the coupling term  $\boldsymbol{\iota}$  in the outer loop subsystem temporarily, namely

$$\mathbf{f}_a = [0, 0, 0]^\top \Rightarrow \boldsymbol{\iota} = \mathbf{0}_{12 \times 1} \quad (35)$$

then, the error dynamics of the outer loop subsystem can be reexpressed as

$$\dot{\mathbf{e}} = \kappa(\mathbf{e}, \mathbf{f}_{ou}, \boldsymbol{\alpha}_d). \quad (36)$$

*Theorem 1:* Based on the proposed control scheme (32), for the error system depicted by (36), the equilibrium point converges to zero asymptotically, i.e.,

$$\lim_{t \rightarrow \infty} \left[ \mathbf{e}_\alpha^\top, \boldsymbol{\Theta}^\top, \dot{\mathbf{e}}_\alpha^\top, \dot{\boldsymbol{\Theta}}^\top \right]^\top = [\mathbf{0}_{4 \times 1}^\top, \mathbf{0}_{2 \times 1}^\top, \mathbf{0}_{4 \times 1}^\top, \mathbf{0}_{2 \times 1}^\top]^\top.$$

*Proof:* To prove *Theorem 1*, choose (30) as the Lyapunov function candidate. Substituting (32) into (31) and noticing (35) in this subsection, one can conclude that

$$\begin{aligned}\dot{V} &= \dot{\mathbf{e}}_\alpha^\top \left( \mathbf{f}_{ou} - [0, 0, (M+m)g, -mg]^\top + K_p \mathbf{e}_\alpha \right) \\ &= -\dot{\mathbf{e}}_\alpha^\top K_d \dot{\mathbf{e}}_\alpha - \dot{\mathbf{e}}_\alpha^\top K_s \left( \dot{\theta}_x^2 + \dot{\theta}_y^2 \right) \dot{\mathbf{e}}_\alpha \\ &= -\left( k_{dx} + k_{sx} \left( \dot{\theta}_x^2 + \dot{\theta}_y^2 \right) \right) \dot{x}^2 \\ &\quad -\left( k_{dy} + k_{sy} \left( \dot{\theta}_x^2 + \dot{\theta}_y^2 \right) \right) \dot{y}^2\end{aligned}$$

$$\begin{aligned} & - \left( k_{dz} + k_{sz} (\dot{\theta}_x^2 + \dot{\theta}_y^2) \right) \dot{z}^2 \\ & - \left( k_{dl} + k_{sl} (\dot{\theta}_x^2 + \dot{\theta}_y^2) \right) \dot{l}^2 \leq 0 \end{aligned} \quad (37)$$

which indicates that the closed-loop system is Lyapunov stable at the origin. Therefore, from (28)–(30) and (33), the following conclusion is derived<sup>1</sup>:

$$e_x, e_y, e_z, e_l, \dot{e}_x, \dot{e}_y, \dot{e}_z, \dot{e}_l, \dot{\theta}_x, \dot{\theta}_y, f_s \in \mathcal{L}_\infty. \quad (38)$$

Subsequently, the proof of *Theorem 1* will be completed with the aid of LaSalle's Invariance theorem [39]. Define the invariant set  $\Lambda$  as

$$\Lambda = \left\{ (e_x, e_y, e_z, e_l, \dot{e}_x, \dot{e}_y, \dot{e}_z, \dot{e}_l, \theta_x, \theta_y, \dot{\theta}_x, \dot{\theta}_y) \mid \dot{V}(t) = 0 \right\}$$

and let  $\Gamma$  be the largest invariant set in  $\Lambda$ . According to (37), in the largest invariant set  $\Gamma$ , one can draw the following conclusion:

$$\dot{e}_x = \dot{e}_y = \dot{e}_z = \dot{e}_l = 0 \quad (39)$$

and combining with the fact  $\dot{x}_d = \dot{y}_d = \dot{z}_d = \dot{l}_d = 0$ , it can be derived that

$$\dot{x} = \dot{y} = \dot{z} = \dot{l} = 0. \quad (40)$$

Taking the time derivative of (40) yields

$$\ddot{x} = \ddot{y} = \ddot{z} = \ddot{l} = 0. \quad (41)$$

Then, integrating (39) with respect to time, one has

$$e_x = \beta_x, e_y = \beta_y, e_z = \beta_z, e_l = \beta_l \quad (42)$$

where  $\beta_x, \beta_y, \beta_z$ , and  $\beta_l \in \mathbb{R}$  represent the undetermined constants. Substituting (42) into (32), one can obtain that

$$f_{vx} = -k_{px}\beta_x \quad (43)$$

$$f_{vy} = -k_{py}\beta_y \quad (44)$$

$$f_{vz} = -k_{pz}\beta_z + (M + m)g \quad (45)$$

$$f_l = -k_{pl}\beta_l - mg. \quad (46)$$

Substituting (43)–(45) into (11)–(13), respectively, and noticing (41), the following results are derived:

$$\begin{aligned} & ml \left( \ddot{\theta}_x C_x C_y - \ddot{\theta}_y S_x S_y - \dot{\theta}_x^2 S_x C_y - \dot{\theta}_y^2 S_x C_y - 2\dot{\theta}_x \dot{\theta}_y C_x S_y \right) \\ & + ml\dot{\theta}_x C_x C_y - ml\dot{\theta}_y S_x S_y = -k_{px}\beta_x \end{aligned} \quad (47)$$

$$ml\dot{\theta}_y C_y + ml \left( \ddot{\theta}_y C_y - \dot{\theta}_y^2 S_y \right) = -k_{py}\beta_y \quad (48)$$

$$\begin{aligned} & ml \left( \ddot{\theta}_x S_x C_y + \ddot{\theta}_y C_x S_y + \dot{\theta}_x^2 C_x C_y + \dot{\theta}_y^2 C_x C_y - 2\dot{\theta}_x \dot{\theta}_y S_x S_y \right) \\ & + ml\dot{\theta}_x S_x C_y + ml\dot{\theta}_y C_x S_y = -k_{pz}\beta_z. \end{aligned} \quad (49)$$

By observing (47)–(49), the following results are obtained:

$$\frac{d}{dt} \left[ l\dot{\theta}_x C_x C_y - l\dot{\theta}_y S_x S_y \right] = -\frac{k_{px}\beta_x}{m} \quad (50)$$

$$\frac{d}{dt} \left[ l\dot{\theta}_y C_y \right] = -\frac{k_{py}\beta_y}{m} \quad (51)$$

<sup>1</sup>If the  $\infty$  norm of  $v$  satisfies  $\|v\|_\infty \leq \infty$ , then we say that  $v$  belongs to  $\mathcal{L}_\infty$ , i.e.,  $v \in \mathcal{L}_\infty$

$$\frac{d}{dt} \left[ l\dot{\theta}_x S_x C_y + l\dot{\theta}_y C_x S_y \right] = -\frac{k_{pz}\beta_z}{m}. \quad (52)$$

Integrating both sides of (50)–(52) with respect to time, one has

$$l\dot{\theta}_x C_x C_y - l\dot{\theta}_y S_x S_y = -\frac{k_{px}\beta_x}{m}t + \lambda_x \quad (53)$$

$$l\dot{\theta}_y C_y = -\frac{k_{py}\beta_y}{m}t + \lambda_y \quad (54)$$

$$l\dot{\theta}_x S_x C_y + l\dot{\theta}_y C_x S_y = -\frac{k_{pz}\beta_z}{m}t + \lambda_z \quad (55)$$

where  $\lambda_x, \lambda_y$ , and  $\lambda_z \in \mathbb{R}$  represent undetermined constants. Furthermore, assuming that  $\beta_x \neq 0$ , one can obtain

$$l\dot{\theta}_x C_x C_y - l\dot{\theta}_y S_x S_y \rightarrow \begin{cases} -\infty, \beta_x > 0 \\ +\infty, \beta_x < 0 \end{cases} \text{ when } t \rightarrow \infty. \quad (56)$$

However, the conclusion in (56) obviously contradicts with the results in (38), i.e.,  $\dot{\theta}_x, \dot{\theta}_y \in \mathcal{L}_\infty$ , while  $l, C_x, C_y, S_x, S_y \in \mathcal{L}_\infty$ . In an analogous method, analysis for  $\beta_y$  and  $\beta_z$  can be derived and summarized as follows:

$$\beta_x = 0, \beta_y = 0, \beta_z = 0 \Rightarrow e_x = 0, e_y = 0, e_z = 0. \quad (57)$$

Then, substituting (57) into (53)–(55), one can conclude that

$$l\dot{\theta}_x C_x C_y - l\dot{\theta}_y S_x S_y = \lambda_x \quad (58)$$

$$l\dot{\theta}_y C_y = \lambda_y \quad (59)$$

$$l\dot{\theta}_x S_x C_y + l\dot{\theta}_y C_x S_y = \lambda_z. \quad (60)$$

In addition, utilizing (57), formula (47) and (49) can be rewritten as

$$\ddot{\theta}_x C_x C_y - \ddot{\theta}_y S_x S_y - \dot{\theta}_x^2 S_x C_y - \dot{\theta}_y^2 S_x C_y - 2\dot{\theta}_x \dot{\theta}_y C_x S_y = 0 \quad (61)$$

$$\ddot{\theta}_x S_x C_y + \ddot{\theta}_y C_x S_y + \dot{\theta}_x^2 C_x C_y + \dot{\theta}_y^2 C_x C_y - 2\dot{\theta}_x \dot{\theta}_y S_x S_y = 0. \quad (62)$$

According to the relation of the square of trigonometric function, let (61)  $\times C_x +$  (62)  $\times S_x$ , one has

$$\ddot{\theta}_x C_y - 2\dot{\theta}_x \dot{\theta}_y S_y = 0. \quad (63)$$

Recalling *Assumption 2*, substituting (63) and the results  $\ddot{x} = \ddot{z} = 0, \ddot{l} = 0$  into (15), yields  $mgl S_x C_y = 0$ , and it is clear that

$$S_x = 0 \Rightarrow \theta_x = 0 \Rightarrow \dot{\theta}_x = 0 \Rightarrow \ddot{\theta}_x = 0. \quad (64)$$

Accordingly, with the result in (64), from (59) and (60), one can know that  $\lambda_y \tan \theta_y = \lambda_z$ . Assume  $\lambda_y \neq 0$  first, and it can be seen that  $\theta_y$  is a constant, implying

$$\dot{\theta}_y = \ddot{\theta}_y = 0. \quad (65)$$

While if  $\lambda_y = 0$ , from (59), the conclusion (65) can also be derived. Subsequently, from (16) and the results  $\ddot{x} = \ddot{y} = \ddot{z} = 0, \dot{\theta}_x = 0$ , one has  $mgl C_x S_y = 0$ , which indicates

$$\theta_y = 0. \quad (66)$$

Finally, in view of (41) and (46) and the result  $\dot{\theta}_x = \dot{\theta}_y = 0$ , from (14), the following result is obvious:

$$-k_{pl}\beta_l = 0 \Rightarrow \beta_l = 0 \Rightarrow e_l = 0. \quad (67)$$

As a result, from (57), and (64)–(67), the largest invariant set  $\Gamma$  contains the equilibrium point only, i.e.,

$$\lim_{t \rightarrow \infty} [\mathbf{e}_\alpha^\top, \Theta^\top, \dot{\mathbf{e}}_\alpha^\top, \dot{\Theta}^\top]^\top = [\mathbf{0}_{4 \times 1}^\top, \mathbf{0}_{2 \times 1}^\top, \mathbf{0}_{4 \times 1}^\top, \mathbf{0}_{2 \times 1}^\top]^\top.$$

By invoking LaSalle's Invariance theorem, the proof is completed. ■

Considering the existence of the coupling term  $\iota$  in the system, the aforementioned theorem cannot sufficiently guarantee the stability of the closed-loop system. Hence, in the following part, we will prove that the coupling term obeys a growth restriction condition based on the theory on cascade systems. To this end, we first provide the following property and its proof.

*Property 3:* The virtual control input  $\mathbf{f}_{ou}$  satisfies

$$\|\mathbf{f}_{ou}(\mathbf{e})\| \leq \begin{cases} \varepsilon \|\mathbf{e}\|, & \text{for } \|\mathbf{e}\| \geq \chi \\ \varepsilon \chi, & \text{for } \|\mathbf{e}\| < \chi \end{cases} \quad (68)$$

with  $\chi$  and  $\varepsilon$  being positive constants.

*Proof:* Define  $\varrho_p$  and  $\varrho_d$  as the maximum eigenvalues for control gains  $K_p$  and  $K_d$ , respectively, according to the virtual control scheme, the following result is derived:

$$\begin{aligned} \|\mathbf{f}_{ou}\| &= \left\| -K_p \mathbf{e}_\alpha - K_d \dot{\mathbf{e}}_\alpha \right. \\ &\quad \left. + [0, 0, (M+m)g, -mg]^\top + \mathbf{f}_s \right\| \\ &\leq \|K_p \mathbf{e}_\alpha\| + \|K_d \dot{\mathbf{e}}_\alpha\| \\ &\quad + g \sqrt{M^2 + 2m^2 + 2Mm} + \|\mathbf{f}_s\| \\ &\leq g \sqrt{M^2 + 2m^2 + 2Mm} \\ &\quad + \sqrt{2} \max(\varrho_p, \varrho_d) \|\mathbf{e}\| + \|\mathbf{f}_s\|. \end{aligned}$$

From (38), there exists a constant  $C_i \in \mathbb{R}_+$  satisfying  $\|\mathbf{f}_s\| \leq C_i$ . Therefore, the aforementioned equation can be further scaled to

$$\begin{aligned} \|\mathbf{f}_{ou}\| &\leq g \sqrt{M^2 + 2m^2 + 2Mm} + \sqrt{2} \max(\varrho_p, \varrho_d) \|\mathbf{e}\| + C_i \\ &\leq \sqrt{2} \max(\varrho_p, \varrho_d) \left[ \frac{g \sqrt{M^2 + 2m^2 + 2Mm} + C_i}{\sqrt{2} \max(\varrho_p, \varrho_d)} + \|\mathbf{e}\| \right]. \end{aligned}$$

By setting  $\varepsilon = 2\sqrt{2} \max(\varrho_p, \varrho_d)$ ,  $\chi = \frac{g\sqrt{M^2+2m^2+2Mm+C_i}}{\sqrt{2}\max(\varrho_p,\varrho_d)}$ , the result in (68) can be obtained. ■

*Theorem 2:* The proposed control law (32) and (34) can drive the quadrotor to the desired position, and adjust the cable to the desired state, while suppressing the payload swing, implying the following result:

$$\begin{aligned} \lim_{t \rightarrow \infty} & \left[ \boldsymbol{\alpha}^\top, \dot{\boldsymbol{\alpha}}^\top, \theta_x, \theta_y, \dot{\theta}_x, \dot{\theta}_y, \mathbf{e}_R^\top, \mathbf{e}_\Omega^\top \right]^\top \\ &= [\boldsymbol{\alpha}_d^\top, \mathbf{0}_{4 \times 1}^\top, 0, 0, 0, 0, \mathbf{0}_{3 \times 1}^\top, \mathbf{0}_{3 \times 1}^\top]^\top. \end{aligned}$$

*Proof:* In (35),  $\mathbf{f}_a$  is first set as zero vector, while it is taken into account here. According to (26), (27) and  $f = \mathbf{f}_v^\top R \mathbf{e}_3$ , one can derive the following result:

$$\|\mathbf{f}_a\| = \left\| \frac{f}{\mathbf{e}_3^\top R_d^\top R \mathbf{e}_3} \right\| \|[ (\mathbf{e}_3^\top R_d^\top R \mathbf{e}_3) R \mathbf{e}_3 - R_d \mathbf{e}_3 ] \|=$$

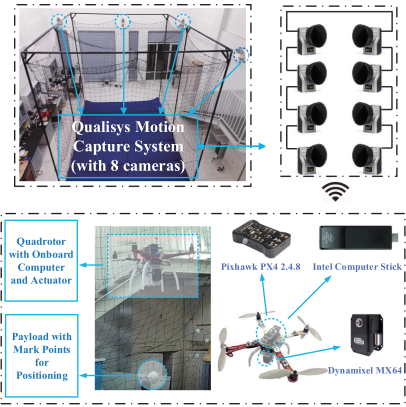


Fig. 5. Experimental platform.

$$\begin{aligned} &= \left\| \frac{f}{\mathbf{f}_v^\top R \mathbf{e}_3} \right\| \|[ (\mathbf{e}_3^\top R_d^\top R \mathbf{e}_3) R \mathbf{e}_3 - R_d \mathbf{e}_3 ] \|= \\ &= \|\mathbf{f}_v\| \|[ (\mathbf{e}_3^\top R_d^\top R \mathbf{e}_3) R \mathbf{e}_3 - R_d \mathbf{e}_3 ] \|. \end{aligned}$$

Based on [38],  $\|[ (\mathbf{e}_3^\top R_d^\top R \mathbf{e}_3) R \mathbf{e}_3 - R_d \mathbf{e}_3 ]\|$  represents the sine of the angle between  $R \mathbf{e}_3$  and  $R_d \mathbf{e}_3$ ,  $\|\mathbf{e}_R\|$  represents the sine of the eigen-axis rotation angle between  $R_d$  and  $R$ , and one can obtain  $\|\mathbf{f}_a\| \leq \|\mathbf{f}_v\| \|\mathbf{e}_R\|$ . Thus, it is implied from (68) that  $\|\mathbf{f}_{au}\| \leq \varepsilon \|\mathbf{e}\| \|\mathbf{e}_R\|$ , for  $\|\mathbf{e}\| \geq \chi$ . Consequently, one can conclude that the coupling term  $\iota$  satisfies the growth restriction condition of  $|\iota| \leq \zeta(\mathbf{e}_R) \|\mathbf{e}\|$ , for  $\|\mathbf{e}\| \geq \chi_\Delta$ , wherein  $\chi_\Delta$  is a positive constant and  $\zeta(\cdot)$  is a class- $\mathcal{K}$  function differentiable at  $[\mathbf{e}_R^\top, \mathbf{e}_\Omega^\top]^\top = \mathbf{0}_{6 \times 1}$ . Subsequently, invoking the theorem on the stability of cascade systems [40], with the results in *Theorem 1* and *Remark 1*, the closed-loop system's equilibrium point is guaranteed to be asymptotically stable. ■

*Remark 2:* Under our current control framework, it is difficult to analyze the robustness of the proposed control schemes (32) and (34) against external disturbances through rigorous mathematical proof, so practical experiment is provided to verify the robustness of the system by applying external disturbances to the system in Section IV. Theoretical analysis of the system's robustness against external disturbances will be focused in our future studies.

## IV. EXPERIMENTAL IMPLEMENTATION AND RESULTS

To evaluate the performance of the aerial transportation system with a manually mounted payload hoisting/lowering device and the proposed control algorithm, in this section, two groups of experiments are conducted.

### A. Experimental Platform

The experiments are carried out on a self-built testbed as shown in Fig. 5. The devised transportation platform is composed of a quadrotor with a mechanism for adjusting the relative motion of the payload. The 2216-KV950 brushless motors with a 30-A electronic speed control (ESC) provide flight power for the quadrotor with wingspan of 450mm. A PixHawk-based flight control unit is connected to the onboard computer through a

**TABLE II**  
QUANTITATIVE DATA

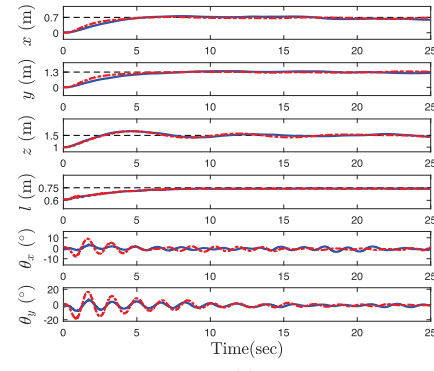
Exp1-T1	The proposed method	The PD controller
$\Theta_{\max}^{\top}$ (°)	[2.87, 8.44]	[8.62, 19.35]
Exp1-T2	The proposed method	The PD controller
$\Theta_{\max}^{\top}$ (°)	[1.46, 9.20]	[8.88, 17.60]

MAVROS-based communication protocol. The mechanism for adjusting the cable length is formed by a Dynamixel MX-64 actuator, a 3-D-printed quadrotor–actuator connector, and a 3-D-printed spool. The spool is connected to the actuator to coil the cable. The actuator is fixed beneath the quadrotor through the 3-D-printed connector controlled by the onboard computer through a serial communications module. The Intel onboard computer runs the 64-bit Ubuntu 16.04 operating system and connects to the ground station via WiFi with the 5G band. The ground station sends the desired position of the quadrotor and cable length to the onboard computer, where the inner loop and the outer loop control programs run. Qualisys motion capture system with eight cameras is used to identify the markers on the quadrotor and the payload, so as to calculate the translational motion of the quadrotor, the cable length, and the swing angles. Then, through WiFi, the observed information is fed back to the outer loop subsystem. Besides, the inertial measurement unit (IMU) information is fed back to the inner loop subsystem. The whole system runs with the support of the robot operating system (ROS).

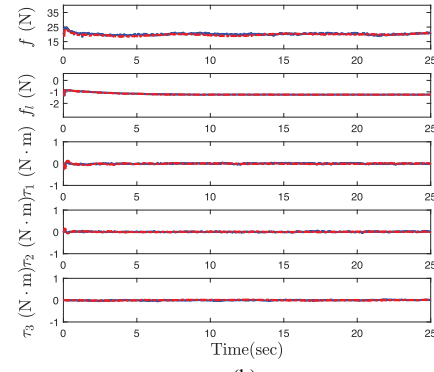
The physical parameters of the experimental platform are given as  $M = 1.74 \text{ kg}$ ,  $m = 0.135 \text{ kg}$ ,  $g = 9.8 \text{ m/s}^2$ , and  $J = \text{diag}([0.0504, 0.0518, 0.0628]) \text{ kg} \cdot \text{m}^2$ . Before the experimental implementation, some numerical simulation tests are performed to verify the performance of the control scheme and direct the experiment process. The control gains are chosen as follows:  $K_p = \text{diag}([2.3, 2.3, 8.0, 3.0])$ ,  $K_d = \text{diag}([5.8, 5.8, 13.2, 4.0])$ ,  $K_s = \text{diag}([2.6, 2.6, 0.8, 0.6])$ ,  $K_R = \text{diag}([1.92, 1.92, 1.92])$ , and  $K_{\Omega} = \text{diag}([0.3, 0.3, 0.3])$ . Besides, the classical PD controller is chosen as the comparison method, whose control gains are set as  $K_p = \text{diag}([4.0, 4.0, 8.0, 3.0])$  and  $K_d = \text{diag}([6.5, 6.5, 13.2, 4.0])$ , and the inner loop control gains are the same as the aforementioned ones. Subsequently, the basic performance and robustness tests, as well as the function and task tests, are verified on the experimental platform.

### B. Experiment Group 1 (Basic Performance and Robustness Tests)

The control objective is to drive the quadrotor to the desired position and adjust the cable to the required length, while suppressing the payload swing simultaneously. Next, two tests are implemented to verify the basic control performance and the robustness against external disturbances. The experimental results are recorded by Figs. 6 and 8, and the explicit quantified data on maximum payload swing angles  $\Theta_{\max}$  are collected by Table II.



(a)



(b)

**Fig. 6.** Results for Exp1-T1. (Blue solid lines: Results by the proposed method. Red dotted lines: Results by the PD method.) (a) Quadrotor position, cable length and payload swing angles. (b) Control inputs.

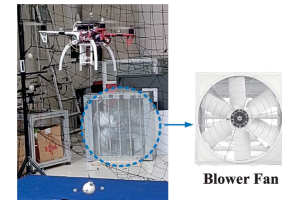
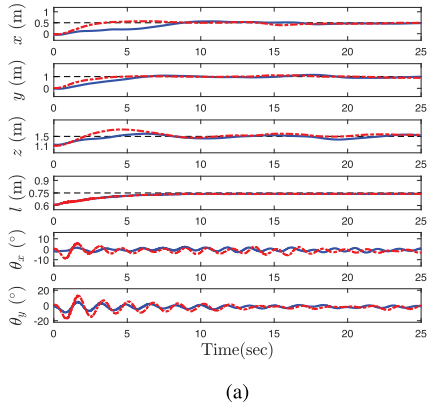


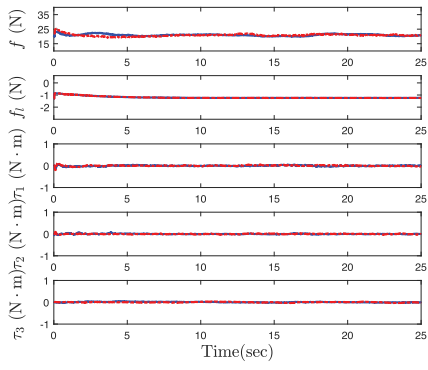
**Fig. 7.** Wind disturbance test platform.

**1) Test 1:** The initial and the desired states of the quadrotor and the cable are set as  $\alpha_0^{\top} = [0.0, 0.0, 1.0, 0.6] \text{ m}$  and  $\alpha_d^{\top} = [0.75, 1.3, 1.5, 0.75] \text{ m}$ , respectively. The obtained experimental results are illustrated in Fig. 6, from which one finds that both schemes can drive the quadrotor to the desired position with similar transportation efficiency. Meanwhile, with the help of the manually mounted payload hoisting/lowering device, the cable length converges to the desired value accurately. From Fig. 6 and Table II, the maximum payload swing angle  $\Theta_{\max}$  by the proposed method is much smaller than that of the PD-based control method.

**2) Test 2:** In order to validate the control performance in a more realistic environment, in this test, we applied a continuous wind disturbance to the system through an air blower. The experimental environment and results are shown in Figs. 7 and 8, respectively. The initial state of the quadrotor and the cable is set as  $\alpha_0^{\top} = [0.0, 0.0, 1.1, 0.6] \text{ m}$  and the desired state is  $\alpha_d^{\top} = [0.5, 1.0, 1.5, 0.75] \text{ m}$ . Define  $\Theta = [\bar{\theta}_x, \bar{\theta}_y]^{\top}$  as



(a)



(b)

**Fig. 8.** Results for Exp1–T2. (Blue solid lines: Results by the proposed method. Red dotted lines: Results by the PD method.). (a) Quadrotor position, cable length, and payload swing angles. (b) Control inputs.

the average of the corresponding absolute value for the swing angles. One can conclude that for the PD controller  $\bar{\Theta} = [2.14^\circ, 3.70^\circ]^\top$ , while for the proposed controller  $\bar{\Theta} = [1.13^\circ, 2.24^\circ]^\top$ . Besides, define  $\bar{e}_\alpha = [\bar{e}_x, \bar{e}_y, \bar{e}_z, \bar{e}_l]^\top$  as the average of the absolute value for the quadrotor positioning and the cable length adjustment error from 15 to 25 s. For the PD controller,  $\bar{e}_\alpha = [0.041, 0.059, 0.059, 0.011]^\top$  m, while for the proposed controller,  $\bar{e}_\alpha = [0.034, 0.079, 0.056, 0.011]^\top$  m. It is obvious that the steady-state errors of the two methods are both satisfactory, while the average of the absolute value for the swing angles is much smaller under the proposed method. Thus, combining with Table II, one can well perceive that although the proposed method sacrifices the positioning speed of the quadrotor to a certain extent, it presents an excellent performance in antiswing compared to the PD controller, and can still drive the system to the desired state in quadrotor positioning and cable length adjusting.

### C. Experiment Group 2 (Function and Task Tests)

Because the designed equipment and control scheme have payload hoisting/lowering ability, the traditional challenging tasks for the fixed-length cable can now be implemented. In this

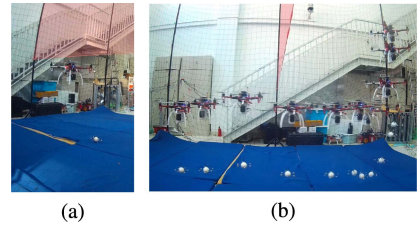
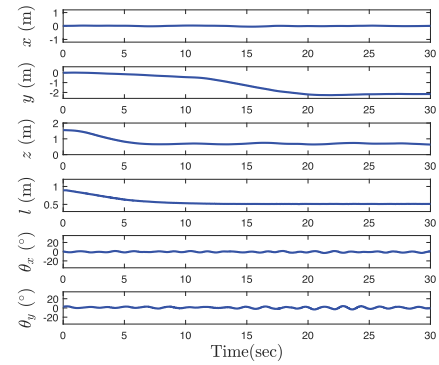
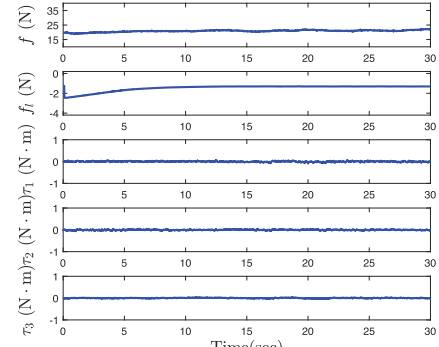


**Fig. 9.** Limited space crossing test. (a) Crossing process of the fixed-length cable. (b) Crossing process of the developed system with varying-length cable. (From right to left.)



(a)



(b)

**Fig. 10.** Results for Exp2–T1. (a) Quadrotor position, cable length, and payload swing angles. (b) Control inputs.

experiment, two tests are conducted for limited space crossing and sample collection.

**1) Test 1 (Limited Space Crossing Test):** When transporting the payload through a small cave or narrow crack, the fixed-length cable may impede the flight. A limited space crossing test is implemented as shown in Fig. 9. However, considering the fixed-length cable case, the quadrotor has to lower its altitude to avoid collision with obstacles, which causes the payload to contact the ground as shown in Fig. 9(a). Yet, the developed system avoids the occurrence of collision risks as presented in Fig. 9(b). At the beginning, the cable length is 0.9 m. To pass through a 0.8-m preset space, the cable needs to be contracted to 0.5 m considering the height of the quadrotor. When the aerial transportation system is approaching the obstacle, the onboard



**Fig. 11.** Sample collection test. The quadrotor first flies over the target, then, the cable stretches to contact with the sample. When the collection work is done, the cable shortens back to its initial length. (From right to left.)

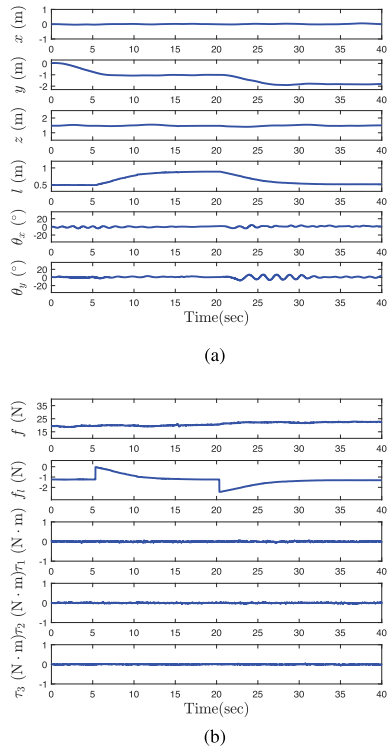


**Fig. 12.** Results for Exp2-T2. (a) Quadrotor position, cable length, and payload swing angles. (b) Control inputs.

computer sends signals to the actuator to hoist the payload to cross through the narrow crack during flight. With the help of the actuator, the limited space crossing task is completed successfully. The states of the system and its inputs are shown in Fig. 10.

**2) Test 2 (Sample Collection Test):** Considering the sampling task, the quadrotor must keep a distance from the surroundings of the target, hence, it is necessary to lengthen the cable before sampling. A simulated sample collection test is shown in Fig. 11. In this test, a magnet is stuck to the bottom of the end effector to draw the sample. At the start, the length of the cable is 0.5 m. When the quadrotor flies over the target, the cable stretches to 0.9 m to contact with the sample. When the collection work is done, the cable shortens to 0.5 m. The corresponding experimental curves are recorded in Fig. 12.

As the actuator device is equipped to the quadrotor UAV, the practical applications of the aerial transportation system are further expanded. The aforementioned experiments clearly

indicate the significance of the developed system. Under the proposed controller, the developed aerial transportation system with flexible connection between the quadrotor and the payload presents superior performance. The system can reach the target position and the desired cable length while eliminating the payload swing. In the designed experimental environment, it can complete both the limited space crossing test and the sample collection work.

*Remark 3:* Based on the basic PX4 code, a conventional method is used to deal with the attitude controller. Through an upper level program, (34) is directly calculated and converted into angular velocity according to the system dynamic model, which is then transmitted to the flight control via MAVROS interface. In addition, the PX4 code can be modified to allow the flight controller to receive torque input directly, which will be treated as an important topic in our future studies to improve the performance of the system.

## V. CONCLUSION

The aerial transportation system capable of hoisting/lowering the payload by changing the length of the suspended cable was developed in this article. With high-state DOFs and complex dynamic couplings, the control objectives of simultaneous quadrotor positioning, payload swing elimination, and hoisting/lowering were realized by the proposed control scheme. Particularly, Lyapunov techniques and LaSalle's Invariance theorem were utilized to guarantee the stability of the closed-loop system. Experimental results demonstrated the performance of the developed system. In the ensuing researches, through the further upgrade of hardware, the cable length could be adjusted according to the height of the crossing space estimated by onboard cameras. The visual techniques and ultra wide band technology will also be used to obtain the payload position, so as to extend the application scope of the system especially in outdoor environments. Besides, we will concentrate on designing more advanced control schemes to take care of disturbances for such underactuated systems, and balance the response speed and antiswing effect of the control system to obtain a better transient performance.

## REFERENCES

- [1] D. Wang, Q. Pan, Y. Shi, J. Hu, and C. Zhao, "Efficient nonlinear model predictive control for quadrotor trajectory tracking: Algorithms and experiment," *IEEE Trans. Cybern.*, vol. 51, no. 10, pp. 5057–5068, Oct. 2021.
- [2] K. Zhang, Y. Shi, and H. Sheng, "Robust nonlinear model predictive control based visual servoing of quadrotor UAVs," *IEEE/ASME Trans. Mechatron.*, vol. 26, no. 2, pp. 700–708, Apr. 2021.
- [3] L. Tang, H. Wang, Z. Liu, and Y. Wang, "A real-time quadrotor trajectory planning framework based on b-spline and nonuniform kinodynamic search," *J. Field Robot.*, vol. 38, no. 3, pp. 452–475, Nov. 2021.
- [4] M. Chen, S. Xiong, and Q. Wu, "Tracking flight control of quadrotor based on disturbance observer," *IEEE Trans. Syst., Man, Cybern., Syst.*, vol. 51, no. 3, pp. 1414–1423, Mar. 2021.
- [5] T.-T. Tran, S. S. Ge, and W. He, "Adaptive control of a quadrotor aerial vehicle with input constraints and uncertain parameters," *Int. J. Control.*, vol. 91, no. 5, pp. 1140–1160, 2018.
- [6] Y. Song, X. Liu, B. Xu, Y. Zhang, and C. Yang, "Disturbance observer-based control of quadrotors with motor response delay and throttle nonlinearity," in *Proc. Int. Conf. Unmanned Aircr. Syst.*, Athens, Greece, Sep. 2020, pp. 182–187.

- [7] V. Ghadiok, J. Goldin, and W. Ren, "Autonomous indoor aerial gripping using a quadrotor," in *Proc. IEEE/RSJ Int. Conf. Intell. Robots Syst.*, San Francisco, CA, USA, 2011, pp. 4645–4651.
- [8] D. Mellinger, Q. Lindsey, M. Shomin, and V. Kumar, "Design, modeling, estimation and control for aerial grasping and manipulation," in *Proc. IEEE/RSJ Int. Conf. Intell. Robots Syst.*, San Francisco, CA, USA, Sep. 2011, pp. 2668–2673.
- [9] J. Thomas, G. Loianno, K. Sreenath, and V. Kumar, "Toward image based visual servoing for aerial grasping and perching," in *Proc. IEEE Int. Conf. Robot. Automat.*, Hong Kong, 2014, pp. 2113–2118.
- [10] S. Kim, H. Seo, S. Choi, and H. J. Kim, "Vision-guided aerial manipulation using a multirotor with a robotic arm," *IEEE/ASME Trans. Mechatron.*, vol. 21, no. 4, pp. 1912–1923, Aug. 2016.
- [11] S. Kim, S. Choi, and H. J. Kim, "Aerial manipulation using a quadrotor with a two DoF robotic arm," in *Proc. IEEE/RSJ Int. Conf. Intell. Robots Syst.*, Tokyo, Japan, Nov. 2013, pp. 4990–4995.
- [12] M. Jafarinassab, S. Sirospour, and E. Dyer, "Model-based motion control of a robotic manipulator with a flying multirotor base," *IEEE/ASME Trans. Mechatron.*, vol. 24, no. 5, pp. 2328–2340, Oct. 2019.
- [13] K. Sreenath, T. Lee, and V. Kumar, "Geometric control and differential flatness of a quadrotor UAV with a cable-suspended load," in *Proc. IEEE 52nd Conf. Decis. Control*, Firenze, Italy, Dec. 2013, pp. 2269–2274.
- [14] L. Qian and H. H. Liu, "Path-following control of a quadrotor UAV with a cable-suspended payload under wind disturbances," *IEEE Trans. Ind. Electron.*, vol. 67, no. 3, pp. 2021–2029, Mar. 2020.
- [15] K. Mohammadi, S. Sirospour, and A. Grivani, "Control of multiple quad-copters with a cable-suspended payload subject to disturbances," *IEEE/ASME Trans. Mechatronics*, vol. 25, no. 4, pp. 1709–1718, Aug. 2020.
- [16] B. Xian, S. Wang, and S. Yang, "Nonlinear adaptive control for an unmanned aerial payload transportation system: Theory and experimental validation," *Nonlinear Dyn.*, vol. 98, no. 3, pp. 1745–1760, Oct. 2019.
- [17] S. Yang and B. Xian, "Energy-based nonlinear adaptive control design for the quadrotor UAV system with a suspended payload," *IEEE Trans. Ind. Electron.*, vol. 67, no. 3, pp. 2054–2064, Mar. 2020.
- [18] X. Liang, H. Lin, P. Zhang, S. Wu, N. Sun, and Y. Fang, "A nonlinear control approach for aerial transportation systems with improved antiswing and positioning performance," *IEEE Trans. Automat. Sci. Eng.*, vol. 18, no. 4, pp. 2104–2114, Oct. 2021.
- [19] K. Guo, J. Jia, X. Yu, L. Guo, and L. Xie, "Multiple observers based anti-disturbance control for a quadrotor UAV against payload and wind disturbances," *Control Eng. Pract.*, vol. 102, Jul. 2020, Art. no. 104560.
- [20] K. Zhao, J. Zhang, D. Ma, and Y. Xia, "Composite disturbance rejection attitude control for quadrotor with unknown disturbance," *IEEE Trans. Ind. Electron.*, vol. 67, no. 8, pp. 6894–6903, Aug. 2019.
- [21] A. Erasmus and H. Jordaan, "Robust adaptive control of a multirotor with an unknown suspended payload," *IFAC-PapersOnLine*, vol. 53, no. 2, pp. 9432–9439, 2020.
- [22] P. J. Cruz and R. Fierro, "Cable-suspended load lifting by a quadrotor UAV: Hybrid model, trajectory generation, and control," *Auton. Robots*, vol. 41, no. 8, pp. 1629–1643, Dec. 2017.
- [23] X. Liang, Y. Fang, N. Sun, and H. Lin, "Dynamics analysis and time-optimal motion planning for unmanned quadrotor transportation systems," *Mechatronics*, vol. 50, pp. 16–29, Feb. 2018.
- [24] J. Potter, W. Singhose, and M. Costelloy, "Reducing swing of model helicopter sling load using input shaping," in *Proc. IEEE 9th Int. Conf. Control Automat.*, Santiago, Chile, Dec. 2011, pp. 348–353.
- [25] J. J. Potter, C. J. Adams, and W. Singhose, "A planar experimental remote-controlled helicopter with a suspended load," *IEEE/ASME Trans. Mechatron.*, vol. 20, no. 5, pp. 2496–2503, Oct. 2015.
- [26] S. Tang and V. Kumar, "Mixed integer quadratic program trajectory generation for a quadrotor with a cable-suspended payload," in *Proc. IEEE Int. Conf. Robot. Automat.*, Seattle, WA, USA, May 2015, pp. 2216–2222.
- [27] Y. Alothman and D. Gu, "Quadrotor transporting cable-suspended load using iterative linear quadratic regulator (iLQR) optimal control," in *Proc. 8th Comput. Sci. Electron. Eng.*, Colchester, U.K., Jan. 2017, pp. 168–173.
- [28] D. Hashemi and H. Heidari, "Trajectory planning of quadrotor UAV with maximum payload and minimum oscillation of suspended load using optimal control," *J. Intell. Robotic Syst.*, vol. 100, pp. 1369–1381, Mar. 2020.
- [29] M. E. Guerrero, D. Mercado, R. Lozano, and C. García, "Passivity based control for a quadrotor UAV transporting a cable-suspended payload with minimum swing," in *Proc. IEEE 54th Conf. Decis. Control*, Osaka, Japan, Dec. 2015, pp. 6718–6723.
- [30] X. Liang, Y. Fang, N. Sun, H. Lin, and X. Zhao, "Adaptive nonlinear hierarchical control for a rotorcraft transporting a cable-suspended payload," *IEEE Trans. Syst., Man, Cybern., Syst.*, vol. 51, no. 7, pp. 4171–4182, Jul. 2021.
- [31] T. Chen and J. Shan, "A novel cable-suspended quadrotor transportation system: From theory to experiment," *Aerospace Sci. Technol.*, vol. 104, 2020, Art. no. 105974.
- [32] R. B. Anderson, J. A. Marshall, and A. L'Afflitto, "Constrained robust model reference adaptive control of a tilt-rotor quadcopter pulling an unmodeled cart," *IEEE Trans. Aerosp. Electron. Syst.*, vol. 57, no. 1, pp. 39–54, Feb. 2021.
- [33] T. Lee, "Geometric control of quadrotor UAVs transporting a cable-suspended rigid body," *IEEE Trans. Control Syst. Technol.*, vol. 26, no. 1, pp. 255–264, Jan. 2018.
- [34] M. Guo, D. Gu, W. Zha, X. Zhu, and Y. Su, "Controlling a quadrotor carrying a cable-suspended load to pass through a window," *J. Intell. Robot. Syst.*, vol. 98, no. 2, pp. 387–401, May 2020.
- [35] N. Sun, Y. Fu, T. Yang, J. Zhang, Y. Fang, and X. Xin, "Nonlinear motion control of complicated dual rotary crane systems without velocity feedback: Design, analysis, and hardware experiments," *IEEE Trans. Automat. Sci. Eng.*, vol. 17, no. 2, pp. 1017–1029, Apr. 2020.
- [36] H. Chen and N. Sun, "Nonlinear control of underactuated systems subject to both actuated and unactuated state constraints with experimental verification," *IEEE Trans. Ind. Electron.*, vol. 67, no. 9, pp. 7702–7714, Sep. 2020.
- [37] R. Miranda-Colorado and L. T. Aguilar, "A family of anti-swing motion controllers for 2D-crane with load hoisting/lowering," *Mech. Syst. Signal Process.*, vol. 133, Aug. 2019, Art. no. 106253.
- [38] T. Lee, M. Leok, and N. H. McClamroch, "Geometric tracking control of a quadrotor UAV on SE(3)," in *Proc. IEEE 49th Conf. Decis. Control*, Atlanta, GA, USA, Dec. 2010, pp. 5420–5425.
- [39] H. K. Khalil, *Nonlinear Systems*. Upper Saddle River, NJ, USA: Prentice-Hall, 2002.
- [40] F. Kendoul, "Nonlinear hierarchical flight controller for unmanned rotorcraft: Design, stability, and experiments," *J. Guid., Control, Dyn.*, vol. 32, no. 6, pp. 1954–1958, May 2009.



**Xiao Liang** (Member, IEEE) received the B.S. degree in intelligence science and technology from the Hebei University of Technology, Tianjin, China, in 2013, and the Ph.D. degree in control theory and control engineering from Nankai University, Tianjin, in 2018.

He is currently an Associate Professor with the Institute of Robotics and Automatic Information System, Nankai University. His research interests include motion planning and nonlinear control of unmanned aerial vehicle systems.



**Hai Yu** received the B.S. degree in automation from Jilin University, Changchun, China, in 2020. He is currently working toward the M.S. degree in control science and engineering with the Institute of Robotics and Automatic Information System, Nankai University, Tianjin, China.

His research interests include nonlinear control of unmanned aerial vehicles.



**Zhuang Zhang** received the B.S. degree in intelligence science and technology from the Hebei University of Technology, Tianjin, China, in 2020. He is currently working toward the M.S. degree in control science and engineering with the Institute of Robotics and Automatic Information System, Nankai University, Tianjin.

His research interests include nonlinear control of multimicro-unmanned aerial vehicles.



**Yongchun Fang** (Senior Member) received the B.S. and M.S. degrees in control theory and applications from Zhejiang University, Hangzhou, China, in 1996 and 1999, respectively, and the Ph.D. degree in electrical engineering from Clemson University, Clemson, SC, USA, in 2002.

From 2002 to 2003, he was a Postdoctoral Fellow with the Sibley School of Mechanical and Aerospace Engineering, Cornell University, Ithaca, NY, USA. He is currently a Professor with the Institute of Robotics and Automatic Information Systems, Nankai University, Tianjin, China. His research interests include nonlinear control, visual servoing, control of underactuated systems, and atomic-force-microscopy-based nanosystems.

Dr. Fang was the recipient the National Science Fund for Distinguished Young Scholars of China. He was an Associate Editor of the *ASME Journal of Dynamic Systems, Measurement, and Control*.



**Huawang Liu** received the B.S. degree in intelligence science and technology from the Hebei University of Technology, Tianjin, China, in 2014, and the M.S. degree in electrical and electronics engineering from the University of Melbourne, Melbourne, Australia, in 2019.

He is currently an Assistant Laboratory Technician with the Institute of Robotics and Automatic Information Systems, Nankai University. His research interests include embedded hardware, firmware for crane, and unmanned aerial vehicle systems.



**Jianda Han** (Member, IEEE) received the Ph.D. degree in mechatronic engineering from the Harbin Institute of Technology, Harbin, China, in 1998.

From 1998 to 2003, he was a Visiting Scientist with the City University of Hong Kong, Hong Kong; Michigan State University, East Lansing, MI, USA; and Cornell University, Ithaca, NY, USA. He is currently a Professor with the Institute of Robotics and Automatic Information Systems, Nankai University, Tianjin, China. His research interests include nonlinear estimation and control, robotics, and mechatronics systems.